

This is the **accepted version** of the article:

Robbennolt, Shauna; Yu, Pengmei; Nicolenco, Aliona; [et al.]. «Magneto-ionic control of magnetism in two-oxide nanocomposite thin films comprising mesoporous cobalt ferrite conformally nanocoated with HfO₂». *Nanoscale*, Vol. 12, Issue 10 (March 2020), p. 5987-5994. DOI 10.1039/C9NR10868H

This version is available at <https://ddd.uab.cat/record/233367>

under the terms of the  ^{IN} COPYRIGHT license

Magneto-ionic control of magnetism in two-oxide nanocomposite thin films comprising mesoporous cobalt ferrite conformally nanocoated with HfO₂

Received 00th January 20xx,
Accepted 00th January 20xx

DOI: 10.1039/x0xx00000x

Shauna Robbenolt,^{*a} Pengmei Yu,^b Aliona Nicolenco,^{a,c} Pau Mercier Fernandez,^a Mariona Coll,^b and Jordi Sort^{*a,d}

Advances in nanotechnology require of robust methods to fabricate new types of nanostructured materials whose properties can be controlled at will using simple procedures. Nanoscale composites can benefit from actuation protocols that involve mutual interfacial interactions on the nanoscale. Herein, a method to create nanoscale composite thin films consisting of mesoporous cobalt ferrite (CFO) whose pore walls are nanocoated with HfO₂ is presented. Porous CFO films are first prepared by sol-gel. Atomic layer deposition is subsequently used to conformally grow a HfO₂ layer at the surface of the pore walls, throughout the thickness of the films. The magnetic properties of uncoated and HfO₂-coated CFO mesoporous films are then modulated by applying external voltage, via magneto-ionic effects. The CFO-HfO₂ composite films exhibit an enhanced magnetoelectric response. The magnetic moment at saturation of the composite increases 56% upon the application of –50 V (compared to 24% for CFO alone). Furthermore, dissimilar trends in coercivity are observed: after applying –50 V, the coercivity of the composite film increases by 69% while the coercivity of the CFO alone decreases by 25%. The effects can be reversed applying suitable positive voltages. This two-oxide nanocomposite material differs from archetypical magneto-ionic architectures, in which voltage-driven ion migration is induced between fully-metallic and oxide counterparts. The synthesized material is particularly appealing to develop new types of magnetoelectric devices with a highly tunable magnetic response.

Introduction

As devices continue to miniaturize, there is an increasing demand for precise methods to fabricate and characterize nanoscale materials, as well as to control their properties at will. While robust methods exist to prepare nanoscale materials, creating solid-state composite materials that are properly mixed at the nanoscale remains a challenge. Nanoporous thin films supported on substrates are ideal for integration into devices because they benefit from the unique nanoscale properties of the material while the substrates allow handling and manipulating them easily on the macroscale. Furthermore, nanoporous thin films with an open pore structure provide the optimal framework to create nanoscale composites if the pores volume is filled with another material.¹⁻⁶

There are several methods that can be used to fabricate nanoporous thin films. These include metal dealloying, sintering micro- or nanoparticles and wet-chemistry techniques.⁷⁻¹⁶ Sol-gel is a method that involves dissolving metal salts into an

oxygen-containing solvent (sol) and allowing the metal ions to bind to the available oxygen creating a network of metal-oxygen bonds (gel). This solution can be deposited onto a substrate and then annealed to form a crystallized metal-oxide film. These films can be made nanoporous by introducing a sacrificial templating agent (e.g., surfactants or micelle-forming polymers) to the solution which is then burned out during annealing leaving an open-cell porous framework. There are many methods that can be used to deposit another material inside the nanoporous framework. Among them, atomic layer deposition (ALD) is one of the most appealing because it uses a gas phase, hence allowing the material to be easily infiltrated and deposited throughout the porous material, not just onto its outer surface.^{3, 6, 17-19}

There is a significant research effort aimed at controlling magnetism on the nanoscale with an applied electric field (converse magnetoelectric effect) with the purpose of enhancing energy efficiency. Traditionally, devices use external magnetic fields to control the magnetic behaviour of materials.

^a Departament de Física, Universitat Autònoma de Barcelona, E-08193 Cerdanyola del Vallès, Spain. E-mail: S.R.: shauna.r@outlook.com, J.S.: jordi.sort@uab.cat

^b Institut de Ciència de Materials de Barcelona (ICMAB-CSIC), Campus UAB, E-08193 Cerdanyola del Vallès, Barcelona, Spain

^c Institute of Applied Physics, MD-2028 Chisinau, Moldova

^d Institució Catalana de Recerca i Estudis Avançats (ICREA), Pg. Lluís Companys 23, E-08010 Barcelona, Spain

†Electronic Supplementary Information (ESI) is available.

These magnetic fields are generated by passing electric current through a wire (e.g., electromagnets). This procedure is unsuitable at the nanoscale due to resistive (Joule) heating energy losses.^{6, 20-22} An alternative to this is to use an applied electric field, not current, to control magnetism. In this case, electrons remain static and no Joule heating effect (due to electrons in movement, i.e., when electric currents are present) takes place. Among the various mechanisms that can result in voltage-driven magnetic actuation, the so-called magneto-ionic effect is one of the most convenient since it typically renders drastic changes in the magnetic properties in films whose thickness is not necessarily limited to few-nm range (as opposed to other mechanisms such as electric surface charge accumulation).^{21,23} Here, ions (typically O^{2-} anions) migrate through the material in response to the applied electric field, hence resulting in variations in the magnetic behavior.²²⁻²⁵ Previously, we demonstrated modulation of the magnetic properties in nanoporous cobalt ferrite (CFO) thin films (without filling the pores with a second phase) via a magneto-ionic mechanism, i.e., due to partial reduction/oxidation reactions.²⁶ Voltage has been also shown to be a very effective means to control the properties of nanoporous Fe_2O_3 , particularly the saturation magnetization.²⁷ In these systems, and also in nanoporous metallic alloys,²⁸ the occurrence of porosity increases the total surface area which is contact with the electrolyte, thus allowing the electric field to be more effectively applied as compared to fully dense films of the same thickness.

In this work, we fabricate a two-phase oxide composite material by means of ALD. This technique is used to deposit a layer of HfO_2 inside the pores of mesoporous CFO thin films previously grown by a sol-gel method. It is observed that, compared to the nanoporous CFO-alone, the nanocomposite films show an enhanced magnetoelectric response. This study differs from most previous works in the literature on magneto-ionics in which the effects are induced in metal/metal oxide bilayer films (not in two-phase oxide thin films).^{22,28,29} In addition, migration of O^{2-} anions is accomplished without need of external heat treatment (in contrast to previous works^{30,31}), hence resulting in a highly energy-efficient procedure.

Experimental section

Preparation of porous CFO

Cobalt(II) nitrate hexahydrate (99.99%), iron(III) nitrate nonahydrate (99.999%) and 2-methoxyethanol (99.8%) were purchased from Sigma-Aldrich. Poly(ethylene oxide)-b-Poly(butylene) with Mn: PEO(4800)-PB(5800), was obtained from Polymer Source. All chemicals were used without further purification.

The initial sol-gel solution was prepared following a previously published recipe.³² $Co(NO_3)_2 \cdot 6H_2O$ (220 g) and $Fe(NO_3)_3 \cdot 9H_2O$ (620 mg) were dissolved in 1 mL of 2-methoxyethanol and 1 mL of ethanol. This solution was mixed using magnetic stirring at

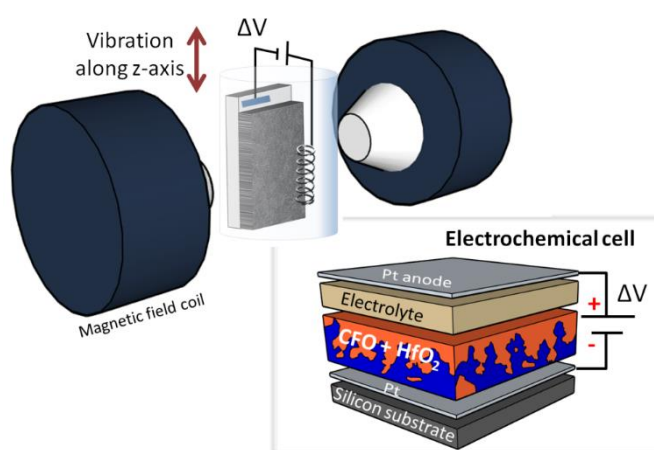


Figure 1. Schematic representation of the *in-situ* application of voltage during magnetic measurements. The Pt layer under the sample is connected as the working electrode and the counter-electrode is a Pt wire. The sample and counter-electrode are in a small Eppendorf tube filled with propylene carbonate treated with Na to remove water (leaving ~ 5 ppm Na^+). The Eppendorf is attached to the sample holder in the VSM which vibrates vertically.

room temperature overnight and was never found to be cloudy at this point. Simultaneously, 10 mg of PEO-PB was dissolved in 1 mL of ethanol and allowed to stir overnight. The next day, the two solutions were combined and allowed to stir for an additional hour. The substrates were prepared by sputtering 70 nm of Pt onto wafers of Si (100). The solution was deposited onto the chips by dip-coating with a withdrawal rate of 300 mm/min after which the samples were transferred to a hot-plate at 80 °C for 10 min. The films were then heated in air to 600 °C for 3 h before cooling to room temperature.

Deposition of HfO_2

The HfO_2 was deposited by ALD using a Cambridge NanoTech Savannah 100 reactor. HfO_2 deposits were prepared by alternate pulsing of tetrakis(dimethylamido)hafnium(IV) (TDMAH) purchased from Sigma-Aldrich and heated at 75 °C and miliQ water as co-reactant. High purity nitrogen gas was used as carrier and purging gas (20 sccm). The chamber temperature was set at 200 °C. Film thickness was set to 7 nm by modifying the number of the ALD cycles and was validated by X-ray reflectivity measurements on silicon (100) reference samples. X-ray diffraction (XRD) was used to check the amorphicity of HfO_2 .

Characterization

High-resolution transmission electron microscopy (HRTEM) images and selected area electron diffraction patterns (SAED) were acquired using a JEM-2011 microscope operating at 200 kV using a CCD Gatan camera. Cross sections were prepared mechanically. The magnetic properties were measured using a MicroSense (LOT-QuantumDesign) vibrating sample magnetometer (VSM). The voltage was applied *in-situ* using an

Agilent B2902A power supply. Figure 1 shows a schematic of the electrochemical cell that was built to be used during VSM measurements. Briefly, the sample and a Pt counter-electrode were placed in an Eppendorf tube and then filled with an anhydrous liquid electrolyte (i.e., propylene carbonate treated with metallic sodium to remove any traces of water). This left a small amount of Na^+ and OH^- ions (≈ 5 ppm Na^+ as determined by inductively coupled plasma (ICP) spectroscopy). The use of a liquid electrolyte is advantageous because it allows the generation of ultra-high electric fields (of the order of hundreds of MV/cm), without electric pinholes, by applying moderate (a few V) voltages.²⁸ Such large electric field is created due to the ultra-small thickness of the electric double layer (typically below 2 nm) that forms around the pore walls when voltage is applied.³³ All magnetic measurements were acquired in an in-plane configuration at room temperature.

Results and discussion

Nanoporous thin films of cobalt ferrite (CFO) with a thickness of 130 nm were deposited on Pt-coated Si substrates ($1 \times 3 \text{ cm}^2$) by dip coating and then a thin layer of HfO_2 was deposited at the surface of the CFO pore walls via ALD. Figure 2 shows a cross-sectional HRTEM image of the CFO- HfO_2 composite. The porous structure of the films is well evidenced in Figure 2a and 2b, and one can see that a 7 nm layer of HfO_2 was deposited fairly uniformly onto CFO throughout the thickness of the film. Figure 2c shows an HRTEM image in which the crystallographic planes of the CFO are clearly visible. It is worth noting that there are no crystallographic planes seen in the HfO_2 which is likely to be amorphous since the samples were not post-annealed after the HfO_2 deposition. The lack of crystallographic peaks for a 40 nm thick HfO_2 , grown by ALD under the same conditions, was also evidenced by grazing incidence XRD (Supplementary Figure S1).

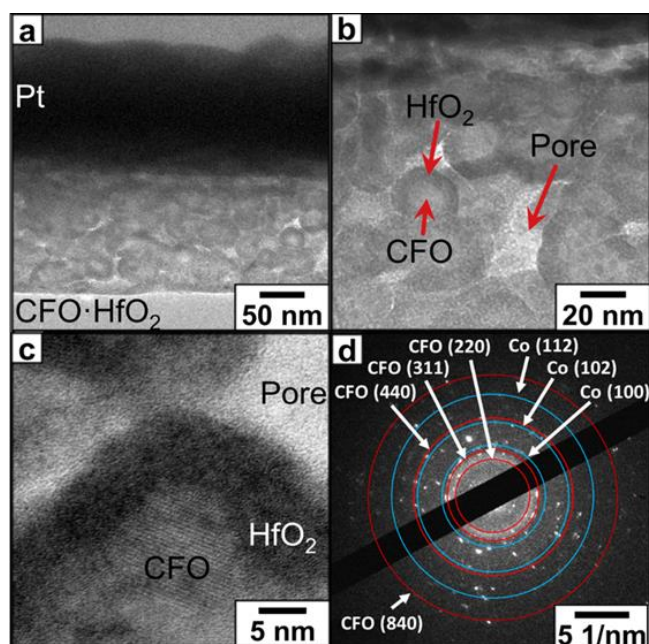


Figure 2. High-resolution transmission electron microscopy images of a cross-section of the composite thin film. Panels a–c show the same film at different magnifications. Panel a is the most zoomed-out and shows the thin film on the Pt layer. Panel b shows the CFO and HfO_2 coating as well as the pore structure. Panel c shows a single ligament where the crystallographic planes of the CFO can be seen surrounded by a thin amorphous HfO_2 nanocoating. Panel d shows the selected area electron diffraction pattern of CFO- HfO_2 after being treated at -50 V. The red rings unambiguously correspond to CFO crystallographic planes, the blue ones to hexagonal Co. The non-indexed spots match reflections of both CFO and Co planes which are virtually superimposed. Indexation of the diffraction peaks was done according to the Crystallography Open Database.

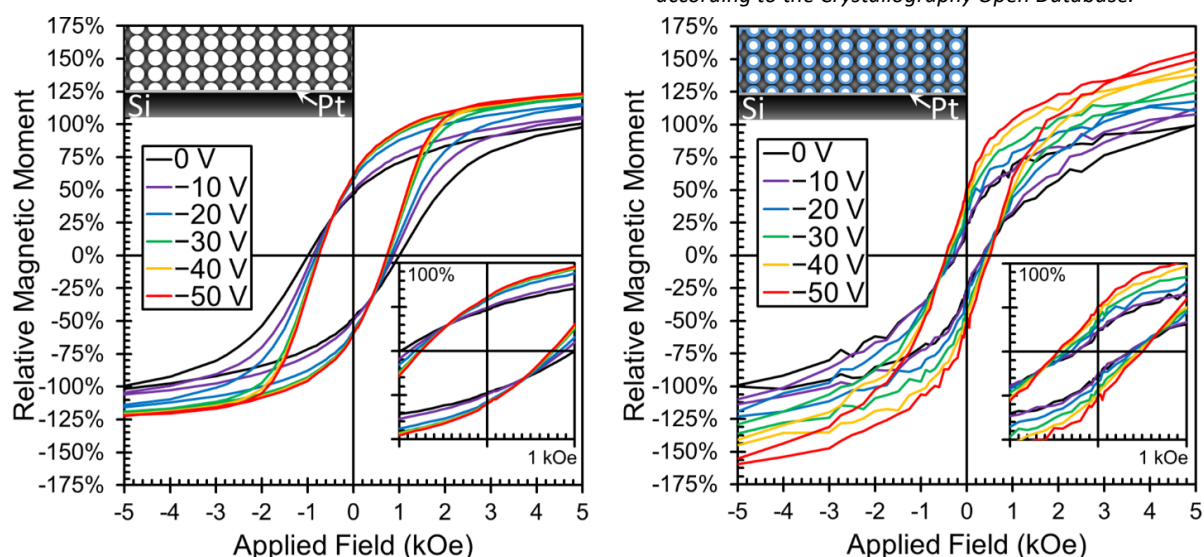


Figure 3. Room-temperature magnetic hysteresis loops of the CFO-alone sample (left) and the CFO- HfO_2 composite (right) as a function of voltage. Each voltage value was applied for 2h. The upper insets are schematic representations of the films. The y-axis is normalized to facilitate comparison between the films and each axis is set such that the magnetic moment at saturation for the initial sample (0 V) is 100%.

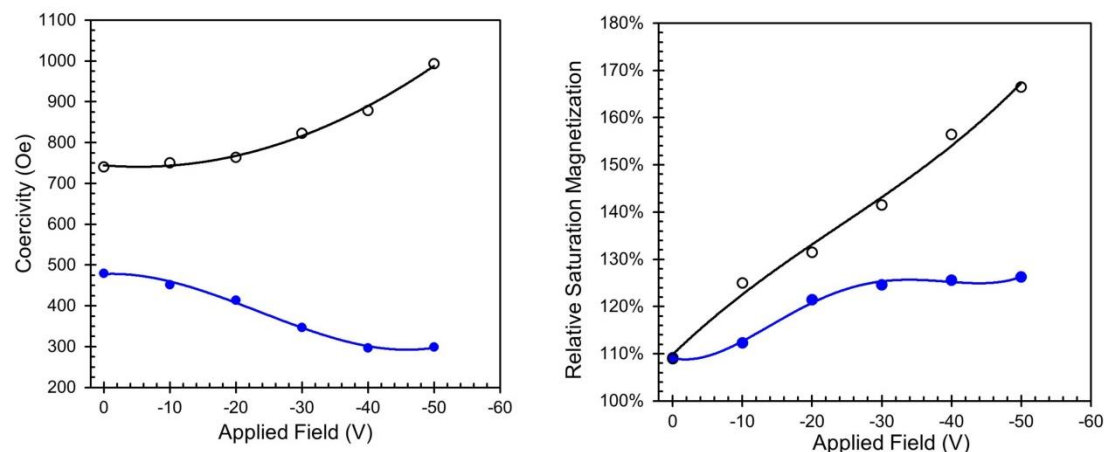


Figure 4. Dependence of the coercivity (left) and relative saturation magnetization (right) on the applied negative voltage extracted from the magnetic hysteresis loops shown in Figure 3. The filled blue symbols represent the trends for the uncoated CFO and the empty black dots correspond to CFO-HfO₂ composite film.

Therefore, eventual ferroelectric properties of HfO₂ (which exist only in the orthorhombic Pca21 crystallographic phase³⁴) can be ruled out. That is, any eventual effect due to voltage application cannot be attributed to the coupling between ferroelectric and magnetostrictive (i.e., CFO) phases.

The magnetoelectric response of the as-prepared material was investigated using the setup described above (Figure 1). Figure 3 shows the magnetic hysteresis loops both before (panel a) and after (panel b) the HfO₂ deposition. Figure 4 shows the dependences of coercivity and saturation magnetization as a function of applied voltage. It should be noted that the composite sample was smaller in lateral size than CFO alone and, therefore, it gives a lower magnetic signal during the measurements. This is why the hysteresis loops of the CFO-HfO₂ samples are noisier. To account for this, the y-axes in (a) and (b) were normalized, so that comparison between the effects of voltage in the two samples is easier. Remarkably, the magnetic moment at saturation increases for both films as more negative voltages are applied. From 0 V to -50 V, the magnetic moment at saturation for the CFO-alone sample increases 24% while that of the composite sample increases by 56%. Hence, the ALD process exacerbates the magnetic effects caused by voltage. This is consistent with a magneto-ionic mechanism.²⁶ The formation of reduced metal atoms or metal clusters indeed explains the increase in magnetic moment at saturation seen in both samples when a negative voltage is applied because Co, Fe and CoFe all have higher M_s values than cobalt ferrite. Indeed, the SAED pattern obtained on the CFO-HfO₂ nanocomposite treated at -50 V (Figure 2d) shows the presence of metallic Co (and eventually Fe) phases. Since the magnetoelectric effects (in particular, magneto-ionic) occur mainly at the interface, the treated sample still retains a large fraction of the CFO. Thus, the four labelled red rings in the Figure 2d arise from planes with interatomic distances 2.92 Å, 2.49 Å, 1.46 Å and 0.92 Å, which correspond to the (220), (311), (440) and (840) crystallographic planes of CFO, respectively. Nevertheless, the three blue rings corresponding to the interatomic distances of 2.17 Å, 1.48 Å and

1.06 Å most likely correspond to the (100), (102) and (112) planes of hexagonal-closed packed Co, which are not superimposed to any reflection from CFO. This indicates the formation of metallic Co phase upon the negative voltage application. Additional spots, not indexed in the SAED pattern of Figure 2d, match positions of CFO (sometimes superimposed to Co) reflections. It should be noted that the outer red ring with interatomic distance around 0.92 Å could also be attributed to the (310) crystallographic plane of metallic Fe. However, one should take into account that the energy needed to reduce Fe in the spinel ferrites is larger than that of Co (or Ni).³⁵ In fact, our previous study on magneto-ionic effects of pure (uncoated) CFO films reveal that the oxidation state of Co tends to be more sensitive to that of Fe to the applied electric field.²⁶

Prior to voltage application, the coercivity (H_c) of the composite films is lower than for the CFO-alone sample (see Figure 3), which means that the ALD deposition causes some changes on the magnetic properties of the samples. Grain growth in CFO associated with the ALD heating could lead to a reduction of H_c . However, the single-domain size for CFO was determined to be around 40 nm³⁶ and the average size of the CFO crystallites in our sample is clearly smaller (see Figure 2c). Hence, the changes in H_c after ALD, rather than being due to changes in crystallite size, are probably related to variations in the amount of oxygen vacancies.

In CFO, the presence of oxygen vacancies results in broken oxygen bonds which are linked superexchange interactions, leading to local spin canting and a larger energy associated to magnetization reversal (i.e., higher H_c ^{32,37}). During ALD the amount of surface oxygen vacancies is likely to be decreased both due to the high-temperature treatment in an oxygen-rich atmosphere and the progressive formation of the HfO₂ defects

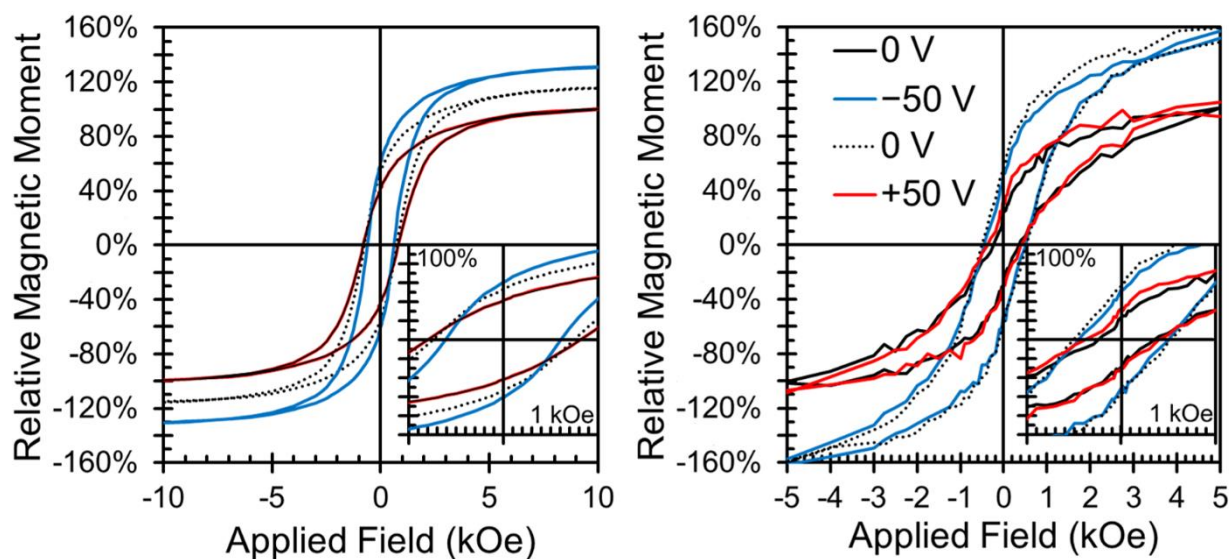


Figure 5. Room-temperature magnetic hysteresis loops of the CFO-alone sample (left) and the CFO-HfO₂ composite (right) showing the reversibility with negative and positive voltages. The measurements were taken in the following order: initial sample (0 V, solid black), after waiting for 90 min at -50 V (blue), 0 V after 14 hours (dotted black), after waiting for 90 min at +50 V. The initial 0 V and the +50 V overlap in the CFO-alone sample. The y-axis is normalized to facilitate comparison between the films and each axis is set such that the magnetic moment at saturation for the initial sample (0 V) is 100%.

in nanoporous CFO would also decrease when CFO becomes chemically bonded to HfO₂.³⁸

nanocoating. This probably leads to the observed reduction of H_c. The surface anisotropy and the amount of surface structural By applying -50 V, the coercivity of the CFO-alone sample decreases from 994 Oe to 741 Oe (25% decrease) while the coercivity of the composite film increases from 295 Oe to 481 Oe (69% increase). This result is to some extent counterintuitive as one might expect the coercivity in both systems to either increase or decrease when the overall oxygen content in the samples is reduced. Indeed, in magneto-ionically manipulated oxide materials that are immersed in electrolytes, the applied negative voltage typically causes O²⁻ ion migration from the sample to the electrolyte and vice versa for positive voltages.^{26,27} The solubility of oxygen in propylene carbonate is rather limited³⁹. Hence, formation of oxygen bubbles could be expected. However, in the voltage window utilized in our experiments, bubbling was not observed. We observed some bubbling in the past during magnetoelectric measurements in other oxide materials (e.g., Co₃O₄) using the same electrolyte but applying much larger voltages, exceeding -200 V. Thus, in the uncoated CFO sample, when negative voltage is applied, O²⁻ ions are likely to be partially released to the propylene carbonate. In turn, upon negative voltages applied in the ALD-coated sample, the O²⁻ ions might migrate from CFO into the structure of HfO₂, which typically contains large amounts of oxygen vacancies in the as-grown state.^{22,34,36-38} Partial migration of O²⁻ ions from HfO₂ to the electrolyte could also occur for strong enough negative voltages.

As the amount of oxygen in CFO decreases, several competing effects will simultaneously occur which might lead to dissimilar trends in coercivity. This makes the interpretation of the overall

dependence of H_c on voltage not straightforward. First, the number of oxygen vacancies in CFO will tend to increase in both systems (uncoated and ALD-coated CFO). This should cause an increase of coercivity.^{32,37} Secondly, magnetic metallic clusters (e.g., Co) form (Figure 2d). Depending on their size, such clusters can be superparamagnetic (with zero coercivity), single-domain (with large coercivity) or multi-domain (with lower coercivity). Thirdly, if partial chemical reduction occurs at the CFO grain boundaries, the effective crystallite size of CFO may decrease (as it was observed in other oxide materials subject to negative voltages²³). Since the size of the CFO crystallites in our mesoporous films is already below the single-domain critical size (40 nm), a further reduction of the crystallite size will tend to reduce H_c.

Depending on which of the effects described above predominates, either an increase or decrease of H_c can occur when negative voltages are applied. Since the amount of oxygen vacancies in the pristine CFO-HfO₂ composite sample is presumably lower than for uncoated CFO (due to the passivation effect induced by HfO₂)⁴⁰, application of voltage is expected to render larger magneto-ionic effects in this case, as observed experimentally. Diffusion of O²⁻ ions from CFO to HfO₂ will create large amounts of oxygen vacancies at the surface of

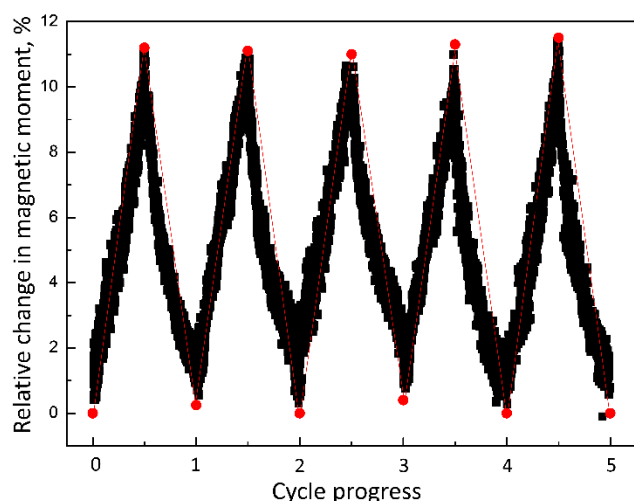


Figure 6. Change in CFO-HfO₂ composite film magnetization (vs. the initial state) during the first 5 cycles measured at 15 kOe. Each cycle took a total of 120 min: 60 min at -10 V followed by 60 min at +10 V. The red line is the trendline and the red dots are the maxima and minima in magnetization.

the CFO pore walls, thereby increasing H_c . However, such O²⁻ vacancies would tend to slightly decrease the saturation magnetization,³⁵ which is not observed experimentally. Therefore, the formation of metallic magnetic clusters (Co and eventually Fe), as confirmed by electron diffraction and the increase of magnetic moment at saturation, is an additional mechanism that plays a role in the coercivity. The larger increase of saturation magnetization in the CFO-HfO₂ compared to uncoated CFO, together with the increase of coercivity for negative voltages, indicate that the fraction of superparamagnetic metallic clusters in the composite film is smaller than for uncoated CFO.

This is in agreement with a more pronounced magneto-ionic effect, which would result in larger metallic clusters in the CFO-HfO₂ composite system. In addition, application of negative voltage to the CFO-HfO₂ composite sample could also cause oxygen to be partially released from HfO₂ to the electrolyte but this should be a second-order effect, which should not drastically influence the resulting magnetic properties of the composite sample since both Hf and HfO₂ are essentially non-magnetic. Namely, while the saturation magnetization of CFO has been reported to be around 455 emu/cm³,⁴¹ some authors have claimed that HfO₂ with large amounts of oxygen vacancies can become slightly ferromagnetic,⁴² with a saturation magnetization of at most 30 emu/cm³ (i.e., at most, 6.5% the value of CFO). Some authors have even ascribed this magnetic moment in HfO₂ to impurities or contamination.⁴³ In any case, the eventual ferromagnetic properties of HfO₂ cannot explain the large variations observed in the magnetic moment at saturation, which exceed 55% for the CFO-HfO₂ sample. Finally, it is possible that the HfO₂ nanocoating could also play a role in induced changes in the mechanical properties of mesoporous CFO when voltage is applied. Namely, the CFO-HfO₂ composite

system may be less able to contract/expand due to electrostriction effects. Voltage-induced strain in the oxygen-deficient CFO could have some influence on the magnetic properties since CFO is magnetostrictive.⁴⁴ However, effects from electrostriction are believed to be a second-order effect and cannot fully explain our results, in particular the drastic changes in magnetization and the dissimilar trends in coercivity. The changes in the magnetic properties induced by applying a negative voltage can be fully reversed with the application of a positive voltage, as shown in Figure 5. The initial hysteresis loop for each sample is shown in solid black lines and the loops after -50 V are shown in blue. For both samples, the voltage was then removed overnight (14 hours) and then a new "0V" loop was measured, shown in dotted black lines. The CFO-alone sample began to recover when the voltage was removed, likely because oxygen stored at the surface or in the solvent had time to begin diffusing back into the sample. However, the changes in the composite sample were permanent and even after 14 hours at 0V, the hysteresis loop matches the loop acquired at -50 V. This suggests that the presence of the HfO₂ layer impedes the migration of oxygen back into the sample either because the oxygen is stable and stored in the HfO₂ or because the oxygen is stored in the electrolyte and the HfO₂ layer physically blocks it from accessing the CFO. Interestingly, after applying +50 V (red lines), both samples recover, and the +50 V loops are almost identical to the initial hysteresis loops. Finally, cyclability experiments (applying -10 V and +10 V several times, consecutively, for 60 min each) were performed (Figure 6) to study the endurance of the investigated effects. Remarkably, within this voltage window, the effects are fully reversible at least during 5 cycles.

Conclusions

Here we have shown that nanoscale cobalt ferrite CFO-HfO₂ composites can be fabricated by using atomic layer deposition to coat nanoporous CFO previously grown using sol-gel methods. Transmission electron microscopy cross-section images reveal that the HfO₂ is deposited uniformly at the surface of the CFO pore walls throughout the film thickness. We then investigated the magnetoelectric properties of both the nanoporous CFO-alone and the CFO-HfO₂ composite. The application of negative voltages induces an increase in the magnetic moment at saturation for both samples while the coercivity is found to decrease in the CFO-alone sample and increase in the nanocomposite. The different magneto-ionic mechanisms responsible for the observed effects are discussed in detail. Furthermore, the changes induced in the composite sample are found to be more permanent than those induced in CFO-alone because the voltage-driven magnetic effects at -50 V remain unaltered after several hours at 0 V. In both types of samples, the initial magnetic properties can be essentially recovered by the application of a positive voltage and a good endurance is demonstrated during voltage cycling experiments. Interestingly, contrary to some other magneto-ionic studies (which require of high temperatures) here all changes in coercivity and saturation magnetization are induced

at room temperature. The large surface area of the investigated material together with the ultra-high electric fields generated due the formation of the very narrow electric double layer,²⁸ are probably the main reasons that allow the magnetoelectric effects to be achieved without need of thermal annealing treatments. These results demonstrate not only that the magnetic properties of nanoporous thin films can be controlled with an electric field, but also that the observed trends in the magnetic parameters can be tailored by creating nanoscale composites and altering the surface oxidation states. This approach might be interesting to design and synthesize spring-magnet materials⁴⁵ via an applied electrical voltage, tuning the relative percentages of soft and hard magnetic phases to achieve an optimum performance (maximized energy products).

Conflicts of interest

There are no conflicts to declare.

Acknowledgements

This work was supported by the European Research Council under the SPIN-PORICS 2014-Consolidator Grant, Agreement No 648454, the Generalitat de Catalunya (2017-SGR-292, 2017-SGR-1519), the Spanish Government (MAT2017-86357-C3-1-R, MAT 2017-83169-R associated FEDER) and the European Union's Horizon 2020 research and innovation programme under the Marie Skłodowska-Curie grant agreement No 665919. P.Y acknowledges Chinese Scholarship Council for CSC fellowship No. 201606920073.

References

- 1 G. J. A. A. Soler-Illia, P. C. Angelomé, M. C. Fuertes, A. Calvo, A. Wolosiuk, A. Zelcer, M. G. Bellino and E. D. Martínez, *J. Sol-Gel Sci. Techn.*, 2011, **57**, 299–312.
- 2 W. Umchoo, C. Sriakkarin, W. Donphai, C. Warakulwit, Y. Poo-arporn, P. Jantaratana, T. Witoon and M. Chareonpanich, *Energ. Convers. Manage.*, 2018, **159**, 342–352.
- 3 J. W. Elam, G. Xiong, C. Y. Han, H. H. Wang, J. P. Birrell, U. Welp, J. N. Hryn, M. J. Pellin, T. F. Baumann, J. F. Poco and J. H. Satcher, *J. Nanomater.*, 2006, **2006**, 64501.
- 4 K. M. Coakley, Y. Liu, M. D. McGehee, K. L. Frindell and G. D. Stucky, *Adv. Funct. Mater.*, 2003, **13**, 301–306.
- 5 J. P. Heremans, C. M. Thrush, D. T. Morelli and M.-C. Wu, *Phys. Rev. Lett.*, 2002, **88**, 216801.
- 6 D. Chien, A. N. Buditama, L. T. Schelhas, H. Y. Kang, S. Robbenolt, J. P. Chang and S. H. Tolbert, *Appl. Phys. Lett.*, 2016, **109**, 112904.
- 7 S. Robbenolt, J. Fornell, A. Quintana, H. Zhang, E. Menéndez, E. Pellicer and J. Sort, *ACS Appl. Mater. Interfaces*, 2018, **1**, 1675–1682.
- 8 B. E. Peecer and J. R. Hampton, *Int. J. Electrochem.*, 2016, **2016**, 2935035.
- 9 J. Zhang and C. M. Li, *Chem. Soc. Rev.*, 2012, **41**, 7016–7031.
- 10 Z. Qi, Y. Gong, C. Zhang, J. Xu, X. Wang, C. Zhao, H. Ji and Z. Zhang, *J. Mater. Chem.*, 2011, **21**, 9716–9724.
- 11 J. C. Thorp, K. Sieradzki, L. Tang, P. A. Crozier, A. Misra, M. Nastasi, D. Mitlin and S. T. Picraux, *Appl. Phys. Lett.*, 2006, **88**, 033110.
- 12 P. Innocenzi and L. Malfatti, *Chem. Soc. Rev.*, 2013, **42**, 4198–4216.
- 13 E. Ortel, T. Reier, P. Strasser and R. Kraehnert, *Chem. Mater.*, 2011, **23**, 3201–3209.
- 14 T. Brezesinski, J. Wang, J. Polleux, B. Dunn and S. H. Tolbert, *J. Am. Chem. Soc.*, 2009, **131**, 1802–1809.
- 15 E. K. Richman, T. Brezesinski and S. H. Tolbert, *Nat. Mater.*, 2008, **7**, 712–717.
- 16 C. Sanchez, C. Boissière, D. Grosso, C. Laberty and L. Nicole, *Chem. Mater.*, 2008, **20**, 682–737.
- 17 M. T. Onn, R. Küngas, P. Fornasiero, K. Huang and J. R. Gorte, *Inorganics*, 2018, **6**, 34.
- 18 M. Ritala, M. Kemell, M. Lautala, A. Niskanen, M. Leskelä and S. Lindfors, *Chem. Vap. Deposition*, 2006, **12**, 655–658.
- 19 C. Detavernier, J. Dendooven, S. Pulinthanathu Sree, K. F. Ludwig and J. A. Martens, *Chem. Soc. Rev.*, 2011, **40**, 5242–5253.
- 20 C. Song, B. Cui, F. Li, X. Zhou and F. Pan, *Prog. Mater. Sci.*, 2017, **87**, 33–82.
- 21 A. Quintana, J. Zhang, E. Isarain-Chávez, E. Menéndez, R. Cuadrado, R. Robles, M. D. Baró, M. Guerrero, S. Pané, B. J. Nelson, C. M. Müller, P. Ordejón, J. Nogués, E. Pellicer and J. Sort, *Adv. Funct. Mater.*, 2017, **27**, 1701904.
- 22 K. Duschek, A. Petr, J. Zehner, K. Nielsch and K. Leistner, *J. Mater. Chem. C*, 2018, **6**, 8411–8417.
- 23 A. Quintana, E. Menéndez, M. O. Liedke, M. Butterling, A. Wagner, V. Sireus, P. Torruella, S. Estradé, F. Peiró, J. Dendooven, C. Detavernier, P. D. Murray, D. A. Gilbert, K. Liu, E. Pellicer, J. Nogués and J. Sort, *ACS Nano*, 2018, **12**, 10291–10300.
- 24 L. Baldrati, A. J. Tan, M. Mann, R. Bertacco and G. S. D. Beach, *Appl. Phys. Lett.*, 2017, **110**, 012404.
- 25 C. Leighton, *Nat. Mater.*, 2019, **18**, 13–18.
- 26 S. Robbenolt, E. Menéndez, A. Quintana, A. Gómez, S. Auffret, V. Baltz, E. Pellicer and J. Sort, *Sci. Rep.*, 2019, **9**, 10804.
- 27 S. Robbenolt, A. Nicolenco, P. Mercier Fernández, S. Auffret, V. Baltz, E. Pellicer, E. Menéndez and J. Sort, *ACS Appl. Mater. Interfaces*, 2019, **11**, 37338–37346.
- 28 C. Navarro-Senent, A. Quintana, E. Menéndez, E. Pellicer and J. Sort, *APL Mater.*, 2019, **7**, 030701.
- 29 A. Molinari, H. Hahn and R. Kruk, *Adv. Mater.*, 2019, **31**, 1806662.
- 30 U. Bauer, L. Yao, A. J. Tan, P. Agrawal, S. Emori, H. L. Tuller, S. van Dijken and G. S. D. Beach, *Nat. Mater.*, 2015, **14**, 174–181.
- 31 Q. Chen, G. Liu, S. Gao, X. Yi, W. Xue, M. Tang, X. Zheng and R.-W. Li, *MRS Commun.*, 2018, **9**, 14–26.
- 32 T. E. Quickel, V. H. Le, T. Brezesinski and S. H. Tolbert, *Nano Lett.*, 2010, **10**, 2982–2988.
- 33 X. Zhou, Y. Yan, M. Jiang, B. Cui, F. Pan and C. Song, *J. Phys. Chem. C*, 2016, **120**, 1633–1639.
- 34 E. D. Grimley, T. Schenk, X. Sang, M. Pešić, U. Schroeder, T. Mikolajick and J. M. LeBeau, *Adv. Electron. Mater.*, 2016, **2**, 1600173.
- 35 S. Anjum, G. H. Jaffari, A. K. Rumaiz, M. S. Rafique and S. I. Shah, *J. Phys. D: Appl. Phys.*, 2010, **43**, 265001.
- 36 X. Tang, L. Jin, R. Wei, X. Zhu, J. Yang, J. Dai, W. Song, X. Zhu and Y. Sun, *J. Magn. Magn. Mater.*, 2017, **422**, 255–261.
- 37 G. Q. Gao, C. Jin, P. Wang, X. Pang, D. X. Zheng and H. L. Bai, *J. Magn. Magn. Mater.*, 2018, **460**, 361–367.
- 38 X. Tang, R. Wei, L. Hu, X. Zhu, J. Yang, J. Dai, W. Song, X. Zhu and Y. Sun, *J. Appl. Phys.*, 2017, **121**, 245305.
- 39 W. R. Baird and R. T. Foley, *J. Chem. Engineer. Data* 17 (1972) 355–357.
- 40 D. Wang, G. He, L. Hao, J. Gao and M. Zhang, *J. Mater. Chem. C*, 2019, **7**, 1955–1965.
- 41 B. X. Gu, *Appl. Phys. Lett.*, 2003, **82**, 3707–3709.
- 42 N. H. Hong, *Phys. Status Solidi (c)*, 2007, **4**, 1270–1275.

- 43 D. W. Abraham, M. M. Frank and S. Guha, *Appl. Phys. Lett.*, 2005, **87**, 252502.
- 44 R. Grössinger, R. S. Turtelli and N. Mehmood, *IOP Conf. Ser.: Mater. Sci. Eng.*, 2014, **60**, 012002.
- 45 G. C. P. Leite, E. F. Chagas, R. Pereira, R. J. Prado, A. J. Terezo, M. Alzamora and E. Baggio-Saitovitch, *J. Magn. Magn. Mater.* 2012, **324**, 2711–2716.